physical sciences forum

MDPI

Proceeding Paper

Bayesian Statistics Approach to Imaging of Aperture Synthesis Data: RESOLVE Meets ALMA †

Łukasz Tychoniec [1,*], Fabrizia Guglielmetti [1], Philipp Arras [2], Torsten Enßlin [2] and Eric Villard [1]

[1] European Southern Observatory, Karl-Schwarzschildstr. 2, D-85748 Garching, Germany
[2] Max Planck Institute for Astrophysics, Karl-Schwarzschild-Str. 1, D-85748 Garching, Germany
* Correspondence: lukasz.tychoniec@eso.org
† Presented at the 41st International Workshop on Bayesian Inference and Maximum Entropy Methods in Science and Engineering, Paris, France, 18–22 July 2022.

Abstract: The Atacama Large Millimeter/submillimeter Array (ALMA) is currently revolutionizing observational astrophysics. The aperture synthesis technique provides angular resolution otherwise unachievable with the conventional single-aperture telescope. However, recovering the image from inherently undersampled data is a challenging task. The `clean` algorithm has proven successful and reliable and is commonly used in imaging interferometric observations. It is not, however, free of limitations. Point-source assumption, central to the `clean` is not optimal for the extended structures of molecular gas recovered by ALMA. Additionally, negative fluxes recovered with `clean` are not physical. This begs the search for alternatives that would be better suited for specific scientific cases. We present recent developments in imaging ALMA data using Bayesian inference techniques, namely the `resolve` algorithm. This algorithm, based on information field theory, has already been successfully applied to image the Very Large Array data. We compare the capability of both `clean` and `resolve` to recover known sky signal, convoluted with the simulator of ALMA observation data, and we investigate the problem with a set of actual ALMA observations.

Keywords: Bayesian inference; inference methods; image analysis; radio astronomy

Citation: Tychoniec, Ł.; Guglielmetti, F.; Arras, P.; Enßlin, T.; Villard, E. Bayesian Statistics Approach to Imaging of Aperture Synthesis Data: RESOLVE Meets ALM. *Phys. Sci. Forum* **2022**, *5*, 52. https://doi.org/10.3390/psf2022005052

Academic Editors: Frédéric Barbaresco, Ali Mohammad-Djafari, Frank Nielsen and Martino Trassinelli

Published: 15 March 2023

1. Introduction

1.1. Aperture Synthesis

The Atacama Large Millimeter/submillimeter Array (ALMA) is revolutionizing observational astrophysics. With its 66 antennas located on the Atacama desert it provided the sharpest ever images of the submillimeter sky, for example, images of the protoplanetary disks at 1 au resolution [1]. In order to obtain such a resolution at a distance to a nearby star-forming region at 1.3 mm a telescope diameter of ∼15 km are needed. Since the construction challenges of such an antenna, especially if one would like to make it steerable, are far beyond current technical capabilities, in radio astronomy domain we often turn to aperture synthesis techniques, where instead of a single dish, a combination of smaller antennas is used, and with interference of signal between each antennas a resolution compared to the a telescope of a size of the greatest distance between the two antennas in an array (i.e., baseline) is achieved.

This does not come without a cost: sampling the baselines is never complete compared with a single dish telescope. This means that we do not receive complete information at all baselines, and thus to create an image of the sky we are operating with missing information.

A direct measurement of an interferometer is the interference pattern between two given antennas. This pattern is related to the sky brightness observed by the antennas. The recorded complex value, referred to as *visibility*, is then a Fourier transform of the sky brightness, the quantity which observations aim to recover. Therefore, a simplified imaging process consists of a (reverse) Fourier transformation of the measured visibilities (while the

non-measured visibilities are set to 0) to obtain first approximation of the sky brightness, the so-called *dirty image* [2,3]. Once this is achieved, it becomes apparent that even with a modern interferometer such as ALMA with many baselines sampling the so-called UV plane we achieve a rather poor quality image. Refining this image presents the topic of this work.

1.2. CLEAN as a Standard Approach to the Imaging of the Interferometric Data

A standard technique to improve the image quality of the interferometric observations was developed by Hogbom in 1974 [4] and is called `clean`. `Clean` exploits the well-defined point-spread function of a given antenna configuration. The algorithm identifies the point sources in an initial dirty image, where the point sources are then approximated with a delta function, convolved with a dirty beam (i.e., the assumed pattern that the point-source would create on the dirty image), scaled with brightness of the suspected point source and the point-source patter is subtracted from the dirty image. This is an iterative process that ideally ends when all point sources are removed from the dirty image until it consists only of noise [2].

One issue of `clean` that can be easily identified is in the assumption that the sky is composed of point sources. This results in `clean` struggling with imaging of extended sky brightness structures. Several modifications to the original `clean` algorithm have been implemented to mitigate this issue, such as multi-scale clean which allows to set a point-source that would be a Gaussian rather than a delta function [5,6].

There are several steps in the process of cleaning which can be modified to improve the process. Masking is a method to restrict an area where the algorithm will search for point sources to a selected region in the sky. Weighting allows us to attribute different weights to different u, v scales, allowing for a trade-off between resolution and sensitivity.

Although `clean` became the gold standard of interferometric data imaging, producing many stunning images of astronomical objects, its limitation beg the search for alternatives, especially in cases where its assumptions are not met.

1.3. `Resolve` Algorithm and IFT

Imaging of the interferometric data can be presented as an inference problem, since we operate on an incomplete measurement problem, trying to find the true sky emission from the received data. Radio Extended SOurces Lognormal deconVolution Estimator `resolve` (https://gitlab.mpcdf.mpg.de/ift/resolve) [5,7] is designed in the Information Field Theory (IFT) framework [8]. IFT enables to use Bayesian inference methods in the context of mathematical framework of field theory. This is well fitted to the issue of imaging the sky brightness. IFT algorithms are implemented in `resolve` through Python package NIFTy (https://gitlab.mpcdf.mpg.de/ift/NIFTy) [9,10].

The measurement equation can be presented as: $d = R(s) + n$, where R is a response of the instrument to the original physical signal (s), and n is noise. In the IFT framework, obtained data d is analyzed in order to find the most probable form of s, which is signal from the field, in this case, the sky. This takes the form of Bayes' theorem:

$$P(s|d) = \frac{P(d|s)P(s)}{P(d)}, \tag{1}$$

$P(d|s)$—likelihood that a given data (d) has been produced from a signal (s), $P(s)$—is a prior knowledge about the signal, and $P(d)$ is a normalization factor.

`Resolve` is developed in order to optimize imaging of extended and diffuse radio sources and to provide reliable noise estimation [5]. It has been successfully used for example in imaging of Cygnus A [11] observed with the VLA and the M87* black hole environment with VLBI [12]. In this work we want to explore `resolve` capabilities for ALMA interferometer, specifically compared with the most commonly used `clean` algorithm.

2. Test Datasets

In this section, we present data used to test interferometric imaging methods: `resolve` and `clean`. We use a simple simulated dataset in order to have a complete control over the input information, as well as the real ALMA observations.

2.1. Simulated Data

In this section, we describe the preparation of the simulated data. The major advantage in using simulated datasets to analyze the imaging procedures is a complete control of the input parameters. We control perfectly the shape and brightness of the sources, as well as configuration and behaviour of the telescope array. On the downside of this approach is the difficulty to realistically model the noise acquired during observation and simplistic assumptions about the sky brightness.

We generate a simple 2D array consisting of five Gaussian components of different brightness, size and position angle. This model is input into the Common Astronomy Software Applications package (CASA; [13]) task `simalma`. This task converts image to the sky model, imposing physical properties to the sky, such as spherical coordinates, pixel dimensions, field-of-view and brightness in physical units. Figure 1 (left) shows the sky model generated with `simalma` task in CASA. Afterwards, the task is simulating observations of the given sky model with ALMA observatory. For this specific case we simulate observations with ALMA configuration C-3 at 230 GHz (ALMA band 6), which results in effective resolution of 0.7″, determined approximately by largest available baseline (distance between two antennas). In the case of C-3 configuration this is ∼500 m.

The `simalma` task returns a calibrated Measurement Set (MS), that consists of complex visibilities. Those visibilities are Fourier transform of the sky brightness, therefore reverse Fourier transformation provides a dirty image of the observed sky. Further on we describe the process of imaging with `resolve` and `tclean`.

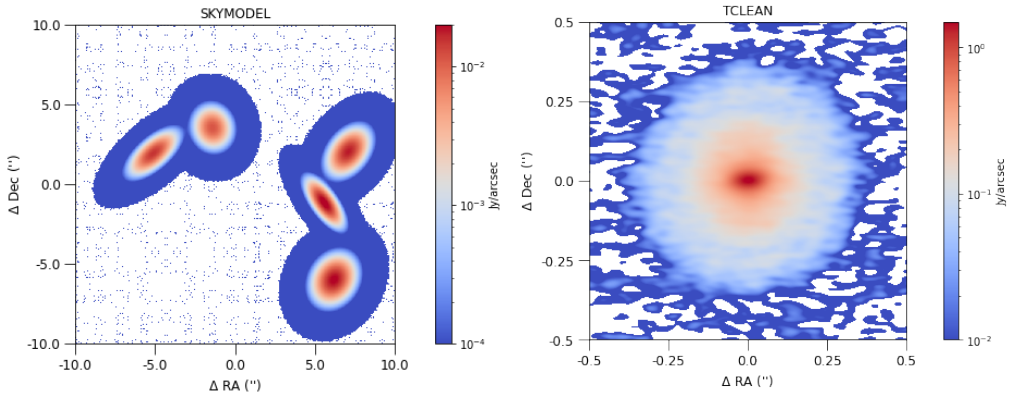

Figure 1. (**Left**) Sky model which serves as an input for creating simulated ALMA Measurement Set. (**Right**) Best `tclean` image of Sz114 protoplanetary disk from ALMA observations.

2.2. ALMA Data

Here, we describe archival ALMA observations used to test application of `resolve` on real-life example. It is important to compare it with a well-understood case, in which the calibration and imaging examples with other tools are already available. We select a protoplanetary disk Sz114 observed within DSHARP ALMA Large Program [14]. This represented a milestone program for the ALMA observatory, showcasing the richness of substructures within disks, often associated with ongoing planet formation. It is therefore especially interesting to search for innovative methods of imaging those data in order to verify current conclusions, as well as open avenues for new studies.

The Sz114 disk shows relatively smooth structure compared with other extreme cases and therefore it serves well as a test case to try to identify underlying structure with

`resolve`. Figure 1 (right) presents image of the disk obtained with `tclean` as delivered by the Large Program team [14].

2.3. Imaging of the Simulated Dataset

First, in order to image the simulated measurement set, we use `tclean` task in CASA software which implements CLEAN algorithm as in Hogbom 1974 [4]. We ran `tclean` without any constraint on where to look for point sources in the image (i.e., without any masking), for 20,000 iterations, or until threshold of 0.3 mJy/beam was reached. Pixel size of the reconstructed image is set to $0.1''$ and image size is set to 512×512 pixels.

This threshold is set based on the earlier, quick `tclean`, so that the algorithm does not attempt to find sources from the residual image consisting purely of noise. In the default settings, weighting of baselines is set to 'natural', which means it associate the baseline with weight proportional to the sampling density (i.e., the most covered baselines have the highest weight). Since there is much more baselines sampling the larger scales, this results in putting more weight to lower resolution, which results in achieving lower resolution than the sky model image. Therefore we also attempt an imaging with Briggs weighting with robust parameter 0.5, which moves the balance of weighting toward longer baselines increasing the resolution but decreasing signal-to-noise ratio. The result of the `tclean` run is presented in Figure 2 (bottom).

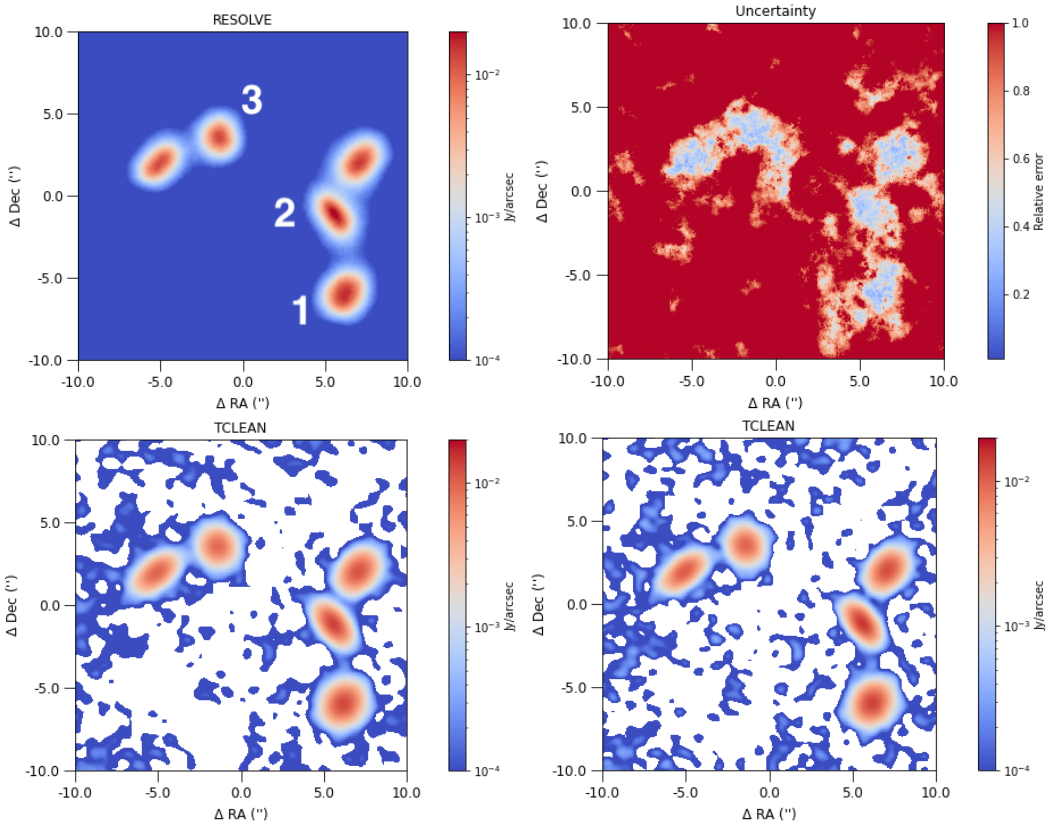

Figure 2. Comparison of the imaging of simulated ALMA observations with `resolve` and `tclean`. (**Top**) `resolve` image (left) with associated uncertainty map. (**Bottom**) two `tclean` images, (Left) with natural weighting; (Right) with Briggs weighting and robust = 0.5.

For `resolve` image of the simulated data we run 30 iterations, using Newton optimizer. We did not make any assumptions on the presence of the point sources in the data. Parameters of the `resolve` run are summarized in Table 1. For detailed explanation of the parameters see Arras et al. [11].

Table 1. Parameters of the `resolve` run on simulated dataset (left) and Sz114 ALMA data (right).

Parameter	Mean	Parameter	Mean
Offset	26	Offset	20
Zero mode	1 ± 0.1	Zero mode	1 ± 0.2
Fluctuations	5 ± 1	Fluctuations	3 ± 1
Power spectrum slope	-2 ± 0.5	Power spectrum slope	-4 ± 2
Flexibility	1.2 ± 0.4	Flexibility	4 ± 0.8
Asperity	0.2 ± 0.2	Asperity	2 ± 0.8

2.4. Imaging of the Real ALMA Observations

For the Sz114 protoplanetary disk observed within DSHARP ALMA Large Program [14], we have created an image from a single spectral window, in order for a direct comparison with `resolve`, which currently does not have the capability to create images of multiple spectral windows. From the publicly available MS file, we extracted spectral window 9 with `split` task in CASA and binned it into a single channel.

For this `tclean` run we implemented both standard and multiscale imaging in order to compare the outcomes, since the observed disk presents large variety of spatial scales. We create images with $0.005''$ and 1024×1024 pixels and run 20,000 iterations up to noise threshold of 0.05 mJy is reached. In the case of multiscale clean, we specified three scales: at 0, 7, and 28 pixels, which means the `tclean` algorithm iterate in order to find three types of sources in the data: either a point source, which corresponds to scale 0, and extended components with Gaussian shape of 7 and 28 pixels of FWHM. Results of the imaging are presented in Figure 3 (bottom).

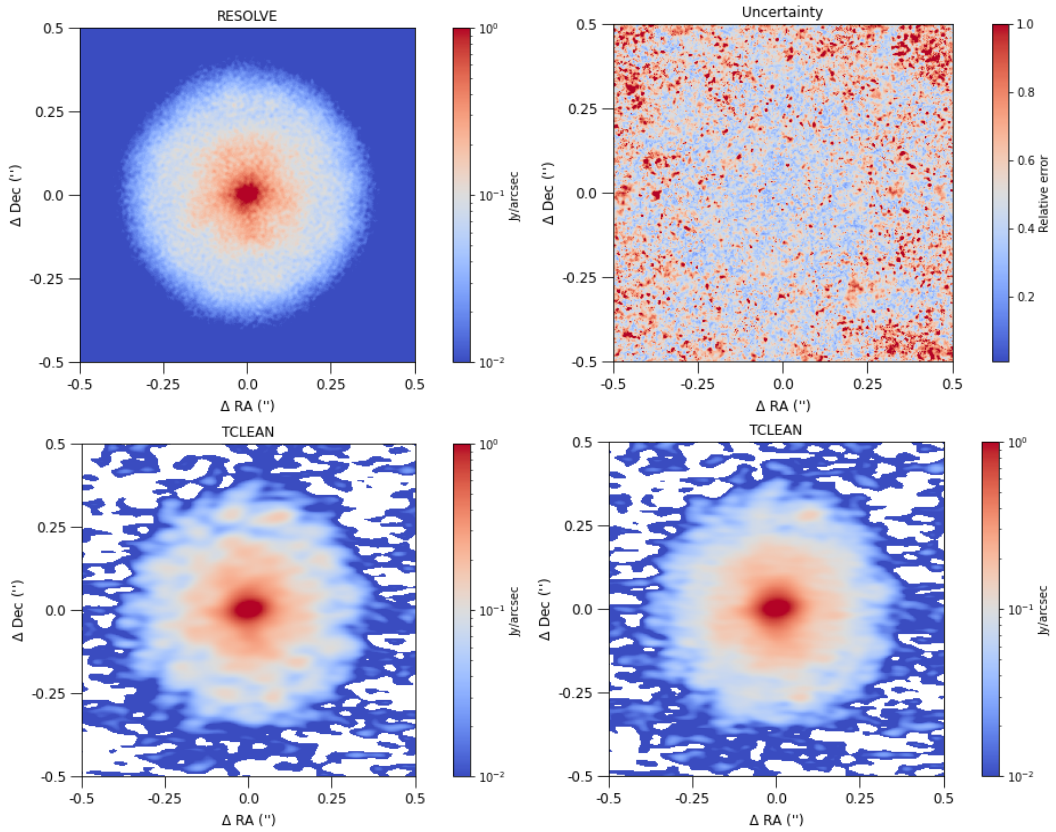

Figure 3. Comparison of the imaging of Sz114 ALMA observations with resolve and tclean. (**Top**) `resolve` image (left) with associated relative error map. (**Bottom**) two `tclean` images, (Left) with standard cleaning algorithm, (Right) with multi-scale algorithm.

A `resolve` imaging followed the same procedure as in the simulated data, however, since the weights were obtained with from real observation, this results in more realistic treatment of the uncertainties. Parameters of this run are shown in Table 1.

3. Comparison between `tclean` and `Resolve`

In this initial study of performance of the `resolve` algorithm in operating with ALMA data, we focus on key aspects of the imaging process: flux recovery—how much flux observed on the sky is recovered by the imaging process and its accuracy; image quality—effective resolution and dynamic range.

3.1. Simulations

We compare the quality of `resolve` and `tclean` imaging of the simple simulated ALMA observation, as described in Section 2.1. Figure 3 presents `resolve` image and associated uncertainty map, and `tclean` image with two different weighting schemes: natural and Briggs weighting with robust parameter of 0.5.

We note that for `tclean` the imaging resulted with large areas with a negative flux, which do not occur in `resolve`—positive-only emission is one of the assumptions in the prior. On the uncertainty map produced by `resolve`, we observe much higher confidence associated with the source positions, compared with positions where no significant emission was detected.

We measure integrated fluxes of each of the Gaussian components in both imaging methods as well as in the input sky model. Result is presented in Table 2. We can note that `resolve` and `tclean` both underestimate the flux of the brightest source (i.e., the Gaussian associated with the largest integrated flux). In case of `tclean`, this can be attributed to imperfect recovery of the signal from the point-spread function, but it is unclear why `resolve` underpredicts the flux. More extensive runs are needed to investigate this issue.

On the other hand, `resolve` reaches good accuracy on the other two measured components. We are able to provide much more reliable error bars on `resolve` by taking the standard deviation of the measured value from all samples in the final iteration.

Table 2. Peak flux (in Jy arcsec^{-2}) of different components on the simulated image.

Comp	Model	`tclean` Natural	`tclean` Briggs	`Resolve`
1	34.11	24.67	24.96	26.68 ± 5.76
2	23.31	21.68	22.19	23.59 ± 6.72
3	16.69	16.31	16.57	17.82 ± 3.86

3.2. ALMA Data

In the case of real ALMA data, it is more difficult to assess total recovered flux since we do not have information on true flux. We compare the peak and total flux integrating over different areas of the disk Table 3. First of all, it can be noted that all `tclean` images have comparable fluxes, and therefore the multiscale did not affect significantly the flux measurements.

Table 3. Peak (in Jy arcsec^{-2}) and integrated flux at given radii of the Sz114 disk.

Radius	Best	`tclean` Hogbom	`tclean` Multiscale	`Resolve`
peak	1.57	1.55	1.49	5.8 ± 3.82
0.06	8.63	8.85	8.95	9.48 ± 1.07
0.15	22.79	22.82	22.53	23.21 ± 0.68
0.35	47.45	47.07	47.24	47.24 ± 2.79

In a comparison between `resolve` and `tclean`, we can see that peak flux measured from `resolve` image is three-times higher than the peak in `tclean` images. This can be purely a gridding effect as the pixel scale of the `resolve` image is much smaller.

At the same time, we note slightly comparable values of the integrated flux measured at from different radii of the disk.

At first sight, it appears that `resolve` is able to create a super-resolution image of the disk. We can use the uncertainty map to understand what confidence can be associated with those structures. We note on the uncertainty map that we typically achieve better than 20% confidence on the results; however, the map also reaches very low confidence in some areas.

4. Conclusions

In this work, we apply Bayesian inference and field theory in the framework of Information Field Theory (IFT) using the `resolve` algorithm, to create images from radio intereferometric observations obtained with ALMA array. The key conclusions are:

- The imaging of simulated ALMA Measurement Set with `resolve` results in successful recovery of the flux of different components in the simulated dataset.
- In one of the first attempts to apply `resolve` on real ALMA data we obtain a high-fidelity image of protoplanetary disk Sz 114, highlighting the potential of `resolve` to create super-resolution images.
- For both test cases, we obtain a robust estimation of the uncertainties on the measured fluxes, which presents one of the major advantages of `resolve` compared with `tclean`.

With these encouraging results, we further highlight areas where exciting developments can be made: `resolve` can be used to create spectral cubes, using correlation between channels as additional prior information; create combined maps of different antenna configuration, a particularly challenging case for `tclean` algorithm and where accurate assessment of the confidence in obtained data is especially necessary.

Author Contributions: Conceptualization, Ł.T. and F.G.; methodology, Ł.T., P.A. and T.E.; software, P.A. and T.E.; data curation, Ł.T.; writing—original draft preparation, Ł.T.; writing—review and editing, F.G., E.V., T.E. and P.A.; project administration, F.G. All authors have read and agreed to the published version of the manuscript.

Funding: This research is supported by an ESO internal ALMA development study investigating interferometric image-reconstruction methods.

Institutional Review Board Statement: The study was conducted according to the guidelines of the ESO internal ALMA Development Studies.

Informed Consent Statement: Not applicable.

Data Availability Statement: This paper makes use of the following ALMA data: ADS/JAO.ALMA 2016.1.00484.L availabile on the ALMA archive https://almascience.eso.org/aq/.

Acknowledgments: This work made use of the following software: resolve [5], matplotlib [15], NIFTy v.8 [16], astropy [17], CASA [13]. This research has made use of NASA's Astrophysics Data System Bibliographic Services. This paper makes use of the following ALMA data: ADS/JAO.ALMA#2016.1.00484.L. ALMA is a partnership of ESO (representing its member states), NSF (USA) and NINS (Japan), together with NRC (Canada), MOST and ASIAA (Taiwan), and KASI (Republic of Korea), in cooperation with the Republic of Chile. The Joint ALMA Observatory is operated by ESO, AUI/NRAO and NAOJ.

Conflicts of Interest: The authors declare no conflict of interest.

References

1. Andrews, S.M.; Wilner, D.J.; Zhu, Z.; Birnstiel, T.; Carpenter, J.M.; Pérez, L.M.; Bai, X.N.; Öberg, K.I.; Hughes, A.M.; Isella, A.; et al. Ringed Substructure and a Gap at 1 au in the Nearest Protoplanetary Disk. *Astrophys. J. Lett.* **2016**, *820*, L40. [CrossRef]
2. Jackson, N. Principles of Interferometry. In *Jets from Young Stars II*; Bacciotti, F., Testi, L., Whelan, E., Eds.; Lecture Notes in Physics; Springer: Berlin/Heidelberg, Germany, 2008; Volume 742, p. 193.
3. Thompson, A.R.; Moran, J.M.; Swenson, G.W., Jr. *Interferometry and Synthesis in Radio Astronomy*, 2nd ed.; John Wiley & Sons: Weinheim, Germany, 2001.
4. Högbom, J.A. Aperture Synthesis with a Non-Regular Distribution of Interferometer Baselines. *Astron. Astrophys. Suppl.* **1974**, *15*, 417.
5. Junklewitz, H.; Bell, M.R.; Enßlin, T. A new approach to multifrequency synthesis in radio interferometry. *Astron. Astrophys.* **2015**, *581*, A59. [CrossRef]
6. Cornwell, T.J. Multiscale CLEAN Deconvolution of Radio Synthesis Images. *IEEE J. Sel. Top. Signal Process.* **2008**, *2*, 793–801. [CrossRef]
7. Arras, P.; Knollmüller, J.; Junklewitz, H.; Enßlin, T.A. Radio Imaging with Information Field Theory. *arXiv* **2018**, arXiv:1803.02174.
8. Enßlin, T.A.; Frommert, M.; Kitaura, F.S. Information field theory for cosmological perturbation reconstruction and nonlinear signal analysis. *Phys. Rev. D* **2009**, *80*, 105005. [CrossRef]
9. Selig, M.; Bell, M.R.; Junklewitz, H.; Oppermann, N.; Reinecke, M.; Greiner, M.; Pachajoa, C.; Enßlin, T.A. NIFTY—Numerical Information Field Theory. A versatile PYTHON library for signal inference. *Astron. Astrophys.* **2013**, *554*, A26. [CrossRef]
10. Arras, P.; Baltac, M.; Ensslin, T.A.; Frank, P.; Hutschenreuter, S.; Knollmueller, J.; Leike, R.; Newrzella, M.N.; Platz, L.; Reinecke, M.; et al. NIFTy5: Numerical Information Field Theory v5. Astrophysics Source Code Library, Record Ascl:1903.008. 2019. Available online: http://ascl.net/1903.008 (accessed on 1 July 2022).
11. Arras, P.; Bester, H.L.; Perley, R.A.; Leike, R.; Smirnov, O.; Westermann, R.; Enßlin, T.A. Comparison of classical and Bayesian imaging in radio interferometry—Cygnus A with CLEAN and resolve. *Astron. Astrophys.* **2021**, *646*, A84. [CrossRef]
12. Arras, P.; Frank, P.; Haim, P.; Knollmüller, J.; Leike, R.; Reinecke, M.; Enßlin, T. Variable structures in M87* from space, time and frequency resolved interferometry. *Nat. Astron.* **2022**, *6*, 259–269. [CrossRef]
13. McMullin, J.P.; Waters, B.; Schiebel, D.; Young, W.; Golap, K. CASA Architecture and Applications. In *Astronomical Data Analysis Software and Systems XVI*; Shaw, R.A., Hill, F., Bell, D.J., Eds.; ASP Conference Series; Astronomical Society of the Pacific: Orem, UT, USA, 2007; Volume 376, p. 127.
14. Andrews, S.M.; Huang, J.; Pérez, L.M.; Isella, A.; Dullemond, C.P.; Kurtovic, N.T.; Guzmán, V.V.; Carpenter, J.M.; Wilner, D.J.; Zhang, S.; et al. The Disk Substructures at High Angular Resolution Project (DSHARP). I. Motivation, Sample, Calibration, and Overview. *Astrophys. J. Lett.* **2018**, *869*, L41. [CrossRef]
15. Hunter, J.D. Matplotlib: A 2D graphics environment. *Comput. Sci. Eng.* **2007**, *9*, 90–95. [CrossRef]
16. Reinecke, M.; Steininger, T.; Selig, M. NIFTy—Numerical Information Field Theory. Available online: https://gitlab.mpcdf.mpg.de/ift/NIFTy (accessed on 1 July 2022).
17. Astropy Collaboration. The Astropy Project: Building an Open-science Project and Status of the v2.0 Core Package. *Astron. J.* **2018**, *156*, 123. [CrossRef]